

When does vapor pressure deficit drive or reduce evapotranspiration?

A. Massmann¹, P. Gentine¹, C. Lin²

¹Department of Earth and Environmental Engineering, Columbia University, New York, NY 10027

²Department of Hydraulic Engineering, Tsinghua University, Beijing, CN

Key Points:

- = enter point 1 here =
- = enter point 2 here =
- = enter point 3 here =

10 **Abstract**

11 = enter abstract here =

12 **1 Introduction**

13 Changes to vapor pressure deficit (VPD) alter the atmospheric demand for water from
 14 the land surface. However, plant stomata have evolved to optimally regulate the exchange
 15 of water and carbon between vegetation and the atmosphere [?]. Therefore, an increase (de-
 16 crease) in VPD may not correspond to an increase (decrease) in evapotranspiration (ET) be-
 17 cause stomatal closure (opening) can cancel the effects of shifts to atmospheric demand.

18 Quantifying the plant response to a perturbation to atmospheric VPD increases our
 19 understanding of feedbacks between the land surface and the atmosphere. If plant response
 20 reduces ET in response to an increase in VPD, the land surface will contribute a positive
 21 feedback in response to atmospheric drying. Conversely, if plant response increases ET in
 22 response to increase in VPD, then the land surface will contribute a negative feedback to
 23 atmospheric drying. The sign of these feedbacks drives the evolution of the atmosphere and
 24 landsurface at many timescales, from diurnal to interdecadal.

25 Here we use a Penman-Monteith framework to quantify plant response to perturbations
 26 to atmospheric demand for water. Section 2 derives the framework, Section 3 describes the
 27 data used, Section 4 presents results, and Section 5 discusses conclusions. The goal of this
 28 paper is to use reasonable approximations as a tool to increase intuition for plant response to
 29 atmospheric drying. This intuition will aid interpretation of observations and full complexity
 30 climate models.

31 **2 Methods**

32 The Penman-Monteith equation (hereafter PM) estimates ET as a function of atmo-
 33 spheric and land-surface variables:

$$34 \quad ET = \frac{\Delta R + g_a \rho_a c_p D_s}{\Delta + \gamma(1 + \frac{g_a}{g_s})}, \quad (1)$$

35 where variable definitions are given in Table 1. ? developed a model for g_s by com-
 36 bining optimal photosynthesis theory with empirical approaches. The result for leaf-scale
 37 stomatal resistance was:

← This section
needs to be
fleshed out,
and I defi-
nitely need
to add more
citations

$$g_{l-s} = g_0 + 1.6 \left(1 + \frac{g_1}{\sqrt{D_s}} \right) \frac{A}{c_s} \quad (2)$$

This can be adapted to an ecosystem-scale stomatal resistance by multiplying by leaf area index (LAI) and converting units to $m s^{-1}$:

$$g_s = LAI \frac{R * T}{P} \left(g_0 + 1.6 \left(1 + \frac{g_1}{\sqrt{D_s}} \right) \frac{A}{c_s} \right) \quad (3)$$

While Equation 3 can be used in PM, it will make analytical work with the function intractable because A is a relatively strong function of ET. To remove dependence of ET on A we can use the semi-impractical results of ?. ? showed that:

$$uWUE = \frac{GPP \cdot \sqrt{D}}{ET} \quad (4)$$

is relatively constant across time and space (within plant functional type). If, following ?, we approximate g_0 as 0, we can use uWUE to remove A from g_s in a way that makes PM analytically tractable:

$$g_s = LAI \frac{R * T}{P} 1.6 \left(1 + \frac{g_1}{\sqrt{D_s}} \right) \frac{uWUE \cdot ET}{c_s \sqrt{D}} \quad (5)$$

Plugging Equation 5 into Equation 1 and rearranging gives:

$$ET = \frac{\Delta R + \frac{g_a P}{T} \left(\frac{c_p D_s}{R_{air}} - \frac{\gamma c_s \sqrt{D}}{LAI R * 1.6 uWUE (1 + \frac{g_1}{\sqrt{D}})} \right)}{\Delta + \gamma} \quad (6)$$

We can then take the derivative with respect to D to determine ecosystem response to atmospheric demand perturbations:

$$\frac{\partial ET}{\partial D} = \frac{g_a P}{T(\Delta + \gamma)} \left(\frac{c_p}{R_{air}} - \frac{\gamma c_s}{LAI 1.6 R uWUE} \left(\frac{2g_1 + \sqrt{D}}{2(g_1 + \sqrt{D})^2} \right) \right) \quad (7)$$

Note that given yearly uWUE from ?, g_1 from ? [as presented in ?], and observations of R , T , P , D_s , and wind speed (WS), the only unknown is LAI. With flux tower observations of ET, LAI will then be uniquely determined for each observation through Equation 6:

$$LAI = - \frac{g_a \gamma c_s \sqrt{D_s} P}{(ET(\Delta + \gamma) - \Delta R - g_a \rho_a c_p D_s) 1.6 R T uWUE (1 + \frac{g_1}{\sqrt{D_s}})} \quad (8)$$

63

Table 1. Definition of symbols and variables

Variable	Description	Units
e_s	saturation vapor pressure	Pa
T	temperature	K
Δ	$\frac{\partial e_s}{\partial T}$	Pa K ⁻¹
R	net radiation at land surface minus ground heat flux	W m ⁻²
g_a	atmospheric conductance	m s ⁻¹
ρ_a	air density	kg m ⁻³
c_p	specific heat capacity of air at constant pressure	J K ⁻¹ kg ⁻¹
D	VPD	Pa
γ	psychrometric constant	Pa K ⁻¹
g_s	stomatal conductance	m s ⁻¹
g_{l-s}	leaf-scale stomatal conductance	mol m ⁻² s ⁻¹
R^*	universal gas constant	J mol ⁻¹ K ⁻¹
LAI	leaf area index	-
c_s	CO ₂ concentration	μ mol CO ₂ mol ⁻¹ air

^aFootnote text here.

59

This “pseudo-LAI” is some part “true” LAI (a measure of leaf area), and some part

60

model and observational error, including error involving our assumption of constant uWUE.

61

By calculating a unique LAI for each observation we will propagate any model and observa-

62

tional uncertainty forward into our expression for $\frac{\partial ET}{\partial D}$.

64

3 Data

65

We use data from FLUXNET2015. Because g_1 coefficients [?] and uWUE were only

66

both available for five plant functional types (PFTs - see Table 2), only 56 of the 77 sites

67

were used. Figure 1 presents each site and its plant functional type.

72

p

← map needs
to be fleshed
out

73

We restrict our analysis to the daytime (sensible heat $> 5 \text{ W m}^{-2}$ and shortwave radia-

74

tion $> 50 \text{ W m}^{-2}$) when there is no precipitation and the plants are growing (GPP $> 10\%$ of

68 **Table 2.** Plant functional types, their abbreviation, Medlyn coefficient [from ?], and uWfUE [from ?].
 69 Note that units are converted such that the quantities fit into Equations 1-8 with the variables in Table 1.

Abbreviation	PFT	g_1 ($\text{Pa}^{0.5}$)	uWUE ($\mu\text{-mol [C] Pa}^{0.5} \text{ J}^{-1} [\text{ET}]$)
CRO	cropland	183.1	3.80
CSH	closed shrub	148.6	2.18
DBF	deciduous broadleaf forest	140.7	3.12
ENF	evergreen needleleaf forest	74.3	3.30
GRA	grassland (C3)	166.0	2.68

^aFootnote text here.

75 the 95th percentile). Also, because some sites use half hourly data but some use hourly, we
 76 aggregate all data to hourly averages. Only times with good quality control flags are used.

77 4 Results

78 By construction, the variability in the LAI term (Equation 8) contains all model and
 79 observational uncertainties. LAI also has physical meaning corresponding to “true” leaf area,
 80 and we expect that it would be approximately $O(1)$. We can have some confidence in our
 81 framework, including the assumption of constant uWUE, if calculated LAIs are generally
 82 $O(1)$. Figure 2 presents the histogram of calculated LAIs with outliers (lowest and highest
 83 5% percent) and unphysical values ($\text{LAI} < 0$) removed. All remaining LAI values are $O(1)$
 84 which provides confidence in model framework.

85 An additional concern is that the LAI term may in fact be some function of D , in which
 86 case the dependence would need to be accounted for when taking the derivative. Figure 3
 87 plots the joint distribution of LAI and VPD, and shows that LAI is very weakly a function of
 88 VPD. Given this weak dependence, we argue that Equation 7 is a valid approximation for ET
 89 response to D .

90 Before diving into calculated values of $\frac{\partial \text{ET}}{\partial D}$, it is useful to consider the functional
 91 form of Equation 7. There are three terms: a scaling term for the full expression we will call
 92 Term 1 ($\frac{g_a P}{T(\Delta+\gamma)}$), a relatively constant offset we will call Term 2 ($\frac{c_p}{R_{air}}$), and a variable term
 93 we will call Term 3 ($\frac{\gamma c_s}{\text{LAI} 1.6 R \text{ uWUE}} \left(\frac{2g_1 + \sqrt{D}}{2(g_1 + \sqrt{D})^2} \right)$). All variables are positive, so the relative

98 magnitude between Term 2 and Term 3 will determine the sign of the derivative, while Term
 99 1 will scale the expression larger or smaller.

100 In Term 1, $\frac{P}{T} \propto \rho$, so this should vary little relative to g_a and Δ . γ should also be rel-
 101 atively constant. So the scaling term, Term 1, should be primarily a function of g_a and tem-
 102 perature (through the function Δ). While temperature range may vary for PFT, the fucntional
 103 form of Δ will be the same. g_a will vary strongly with PFT due to the importance of surface
 104 roughness. However, the coeffiecent of variability for g_a is relatively constant across PFT.
 105 So, the influence of g_a on the relative (to the mean) variability of Term 1 is approximately
 106 similiar across PFT.

107 Figure 4A shows Term 1 normalized by mean g_a (calcualted for each plant functional
 108 type), and confirms that much of the relative variability of Term 1 is contained in the g_a
 109 term's relative variability. Additionally, the impact of T on the relative variability increases
 110 with increasing g_a .

111 While the relative variability of Term 1 is similiar across PFT, the absolute value of
 112 Term 1 varies strongly across PFT. Figure 4B shows Term 1 evaluated with the mean g_a for
 113 each PFT, and at the range of observed temperatures for each PFT. As expected, for the tree
 114 PFTs (DBF, ENF) Term 1 is much larger and the temperature dependence is much stronger.
 115 Systematic differences in observed temperatures also cause differences in the average mag-
 116 nitude of Term 1. For example, ENF experiences on average colder temperatures and is thus
 117 more likely to have a larger scaling term. Additionally, because $\text{std}(g_a) \propto \overline{g_a}$, the spread of
 118 Term 1 due to g_a variability will be larger, although this is not shown for simplicity. To sum-
 119 marize, the variability of Term 1 will look like Figure 4A for each PFT, but the scale of the x
 120 and y-axis will increase or decrease according to Figure 4B.

125 “just say that vpd effect is approximately linear (except at low VPD), and then say so
 126 we are most concerned about when d et/dvpd is zero, as this is the minima. then you can just
 127 look at this treshold as a function of LAI, uWUE, and g1.”

128 Term 2 minus Term 3 determines the sign and magnitude that the scaling Term 1 is
 129 multiplied by. If we assume that c_s variability is relatively less than LAI and D variability,
 130 then variability within PFT will be solely detminded by LAI and D . Figure 5 shows how (Term
 131 2 - Term 3) varies with D and LAI, as a function of PFT. In Figure 5a lower uWUE and LAI
 132 shift the disrtribution of (Term 2 - Term 3) towards negative values. Additionally, the smaller

133 g_1 , the greater the relative D dependence of of (Term 2 - Term 3). This is observed most
 134 strongly for the ENF PFT, which has the smallest g_1 (74.31).

141 Figure 5b shows the location of the minima of ET, as a function of LAI and D . For
 142 any LAI or VPD less (more) than these curves, Term 2 - Term 3 will be negative (positive).
 143 It is clear that the portion of VPD observations below these curves will be a strong function
 144 of LAI . However, we can see some general trends. For CSH, $\frac{\partial ET}{\partial D}$ should be negative for
 145 the vast majority of observed LAI and VPD. The split appears to be more even among ENF,
 146 GRA, and DBF, and we might expect a greater frequency of positive $\frac{\partial ET}{\partial D}$ for CRO.

147 Table 3 confirms these expectations for PFT behaviour of $\frac{\partial ET}{\partial D}$. For all PFTs except for
 148 CRO, average $\frac{\partial ET}{\partial D}$ is less than zero. However, $\frac{\partial ET}{\partial D}$ evaluated at the average of all variables
 149 (e.g. LAI, T , c_s , D) is only negative for CSH and GRA. And, DBF in addition to CRO expe-
 150 riences $\frac{\partial ET}{\partial D} < 0$ less than half the time. These observations highlight the effect of the non-
 151 linear function in Figure 5: $\frac{\partial ET}{\partial D}$ has a much steeper slope when the function is negative, and
 152 is thus more likely to be large magnitude. n The units of $\frac{\partial ET}{\partial D}$ make it difficult to interpret if
 153 D is even a meaningful contributor to ET's variability. To understand D 's contribution better,
 154 we use a linear approximation and present $\frac{\partial ET}{\partial D}$ multiplied by D 's standard deviation. The
 155 range of D 's contribution to ET's variability ranges between 16 - 20 W m⁻² for all PFTs ex-
 156 cept for CSH, which is about 51 W m⁻². Another meaningful comparison is to $\frac{\partial ET}{\partial R} * std(R)$,
 157 as net radiation generally the driver of ET (cite joe berry here). For all PFTs except for CSH
 158 D contributes between 14.5 - 20.5 % of R 's contribution to variability. For CSH the portion
 159 is much larger, about 44 %. However it is important to note that a linear approximation about
 160 a mean base state is probably not a very good approximation across the range of variability,
 161 so these values are just estimates of D 's contribution to ET's variability.

162 So far, idealized plots and statistics have illuminated the form of $\frac{\partial ET}{\partial D}$ and how it varies
 163 with PFT. Large mean LAI and uWUE shifts CRO and DBF towards positive $\frac{\partial ET}{\partial D}$. How-
 164 ever, the strongly nonlinear funtion of $\frac{\partial ET}{\partial D}$ at $\frac{\partial ET}{\partial D} < 0$ pushes $\frac{\partial ET}{\partial D}$ negative for DBF (it
 165 does not do this for CRO because of CRO's high g_1). ENF's low g_1 value increases the de-
 166 pendence of $\frac{\partial ET}{\partial D}$ on D , and makes the function more strongly nonlinear. This has the side
 167 effect of pushing $\frac{\partial ET}{\partial D}$ negative futher than other PFTs for a given fraction $\frac{\partial ET}{\partial D} < 0$ and
 168 magntiude $\frac{\partial ET}{\partial D}(T, \dots, D)$. GRA shows the opposite behavior; a relatively high g_1 makes
 169 the function more linear, decreasing the magnitude of $\frac{\partial ET}{\partial D}$ for a given fraction $\frac{\partial ET}{\partial D} < 0$
 170 and magntiude $\frac{\partial ET}{\partial D}(T, \dots, D)$ (although g_a and Term 1 also probably have a role in this).

175

Table 3. Statistics of $\frac{\partial ET}{\partial D}$ as a function of PFT.

PFT	$\frac{\partial ET}{\partial VPD}$	$\frac{\partial ET}{\partial D} (\bar{T}, \dots, \bar{D})$	$\frac{\partial ET}{\partial D} (\bar{T}, \dots, \bar{D}) * \text{std}(D)$	$\frac{\frac{\partial ET}{\partial D} (\bar{T}, \dots, \bar{D}) * \text{std}(D)}{\frac{\partial ET}{\partial R} (\bar{T}, \dots, \bar{D}) * \text{std}(R)}$	fraction $\frac{\partial ET}{\partial VPD} < 0$
CRO	0.000853	0.026241	18.523659	0.203022	0.473311
CSH	-0.108234	-0.091526	50.861613	0.439379	0.931660
DBF	-0.012727	0.013794	19.734435	0.164241	0.461674
ENF	-0.034087	0.000706	16.611852	0.148548	0.534425
GRA	-0.019637	-0.000921	16.798083	0.173552	0.631735

^aFootnote text here.

171

Finally, low $uWUE$ of CSH pushes to toward by far the lowest values $\frac{\partial ET}{\partial D}$ (Figure 5). Variability in D accounts for the largest about of ET variability for CSH. For the other PFTs, D contributes less to ET variaibiliyt, but still represents about 15-20 % of R 's contributions to ET variability.

176

4.1 Full observations of $\frac{\partial ET}{\partial D}$

177

Now that we have an intuitive understanding of $\frac{\partial ET}{\partial D}$'s behavior, we are equipped to intepret fully realistic plots of $\frac{\partial ET}{\partial D}$ for each PFT. Figure 6 presents calculated $\frac{\partial ET}{\partial D}$ where, unless otherwise noted, all variables in Equation 7 are allowed to vary. Each column is a different quantity related to $\frac{\partial ET}{\partial D}$, and each row is a different PFT.

181

The full observations generally confirm expectations from Section 4. CRO has the most positive values of $\frac{\partial ET}{\partial D}$, $\frac{\partial ET}{\partial D}$ is almost always negative for CSH, and reponse depends more with the environmental conditions for the other PFTs (especially ENF). Through the columns of Figure 6 we can see the impact of LAI and g_a on the variability of $\frac{\partial ET}{\partial D}$. g_a 's (columns 1 and 3) scaling alters the magnitude considerably. LAI (columns 2 and 3) variability adds a lot of additional noise to the signal of $\frac{\partial ET}{\partial D}$, which is slightly undesirable given LAI's role in representing model and observational uncertainty. However, the general story with the noise appears to match the cleaner signal when LAI is help constant and D_{ETmin} is clearly visible . One exception is possibly with GRA, for which uncertainty is high and causes the full complexity plots (Columns 1 and 2) to not match well with LAI held fixed (Columns 3 and 4).

← I really need to make these pltos better - way too much overlapping of points that hurts the story

192 For ENF and GRA D_{ETmin} does not appear to be only a function of LAI. It turns out
 193 that the site to site variability in γ causes D_{ETmin} to vary, which is not discussed in the pre-
 194 cious section. The impact is observable in both ENF and GRA, but especially for ENF which
 195 has a larger $\frac{\partial^2 ET}{\partial^2 D}$ than the other PFTs.

200 In general the full complexity plots of $\frac{\partial ET}{\partial D}$ match our expectations, even with the large
 201 sensitivity to LAI measures of uncertainty observed in Figure 5. Our LAI-based method of
 202 uncertainty propagation blurs the idealized expectations the most for GRA, and also has a
 203 considerable effect for CRO. We therefore have the most confidence in our conclusion based
 204 on Equation 7 for PFTS CSH, DBF, and ENF, as the full complexity plots with uncertainty
 205 included closely match the story when LAI is held fixed. **see somewhat preferred alternate
 206 figure 7 .

210 5 Conclusions

211 The idealized representation of ET used here is successful in developing intuition for
 212 how ET responds to changes in D . This intuition will aid the community in interpreting ob-
 213 servations and output from sophisticated full complexity climate models.

214 The idealized framework leads to the following general conclusions:

- 215 • Aerodynamic resistance plays an important role of scaling $\frac{\partial ET}{\partial D}$. This is a leading
 216 order effect for observing higher magnitude responses in DBF and ENF.
- 217 • In general, CSH has the most negative (i.e. ET reduced) response to increases in D
 218 (atmospheric drying). So CSH plants will almost always try and conserve water, ef-
 219 fectively reducing ET with dry atmospheric perturbation.
- 220 • CRO has the most positive response (i.e. ET increased) in response to increases in
 221 D . This is consistent with CROs that may be evolved or bred to thrive in non-water-
 222 limited environments.
- 223 • The response is more a function of the environment for DBF, ENF, and GRA. Because
 224 as VPD increases the response is more likely to be positive, if RH is fixed then the
 225 response will be more likely to be positive at warmer T, or if T is fixed the response is
 226 more likely to be positive with decreasing RH.
- 227 • ENF has the strongest dependence on environmental conditions due to its small $g1$.
- 228 • Model and observational uncertainty is highest for GRA and CRO, so conclusions
 229 about those PFTs should be tempered.

← I think I like this more as thinking in terms of T and RH is easier. However, I used the other plot because Fig 5 does not discuss things in terms of temperature, as this would make things more complicated (adding another dimension). I could just include both versions of figure 6 though (using figure 6a as a bridge to figure 6b)

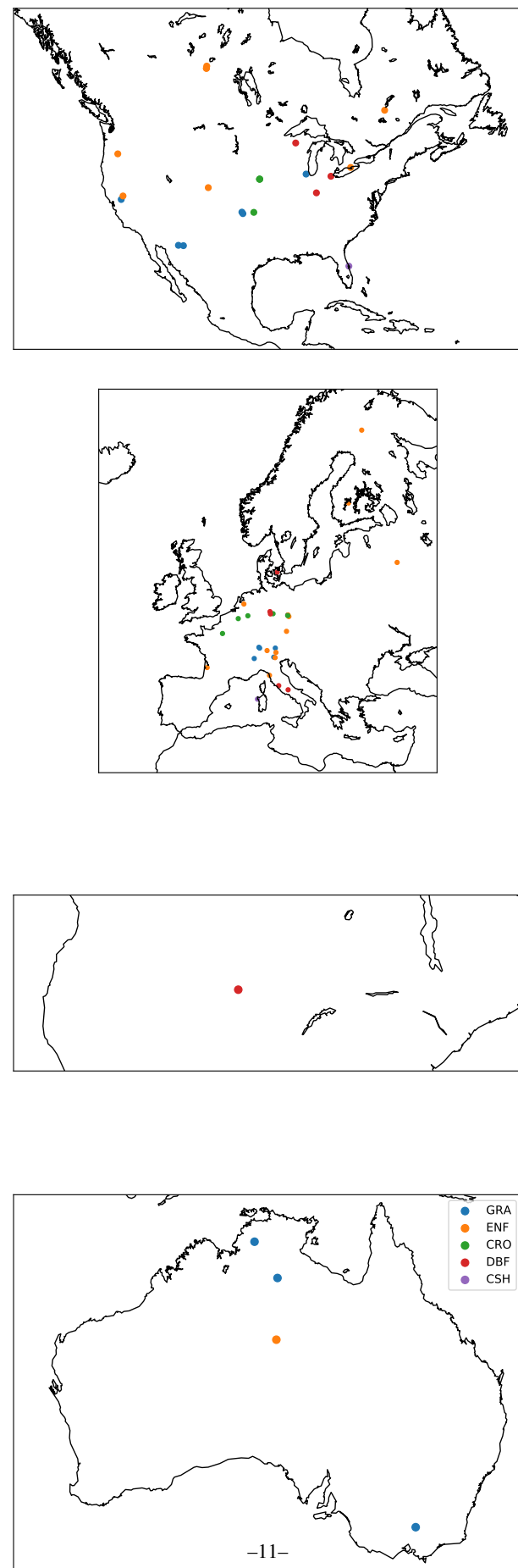
← also need to flesh this section out

- 230 • However, inclusion of uncertainty doesn't alter conclusions about DBF, ENF, and
231 CSH.

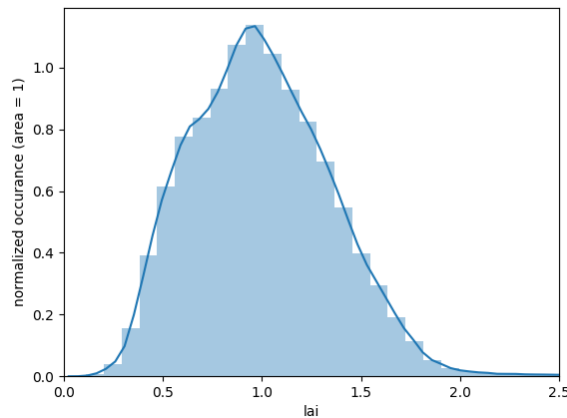
232 The intuition developed using this framework can be used to understand how the land
233 surface will respond and contribute to changes in the environment.

234 **Acknowledgments**

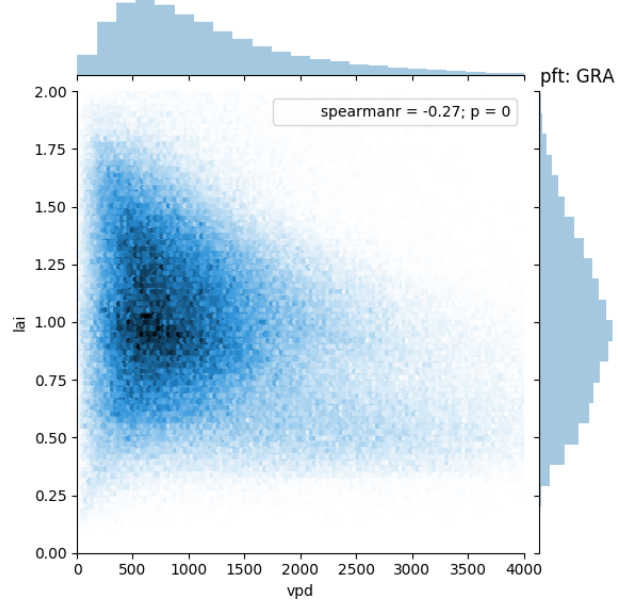
235 This work used eddy covariance data acquired and shared by the FLUXNET community, in-
236 cluding these networks: AmeriFlux, AfriFlux, AsiaFlux, CarboAfrica, CarboEuropeIP, Car-
237 boItaly, CarboMont, ChinaFlux, Fluxnet-Canada, GreenGrass, ICOS, KoFlux, LBA, NECC,
238 OzFlux-TERN, TCOS-Siberia, and USCCC. The ERA-Interim reanalysis data are provided
239 by ECMWF and processed by LSCE. The FLUXNET eddy covariance data processing and
240 harmonization was carried out by the European Fluxes Database Cluster, AmeriFlux Man-
241 agement Project, and Fluxdata project of FLUXNET, with the support of CDIAC and ICOS
242 Ecosystem Thematic Center, and the OzFlux, ChinaFlux and AsiaFlux offices.



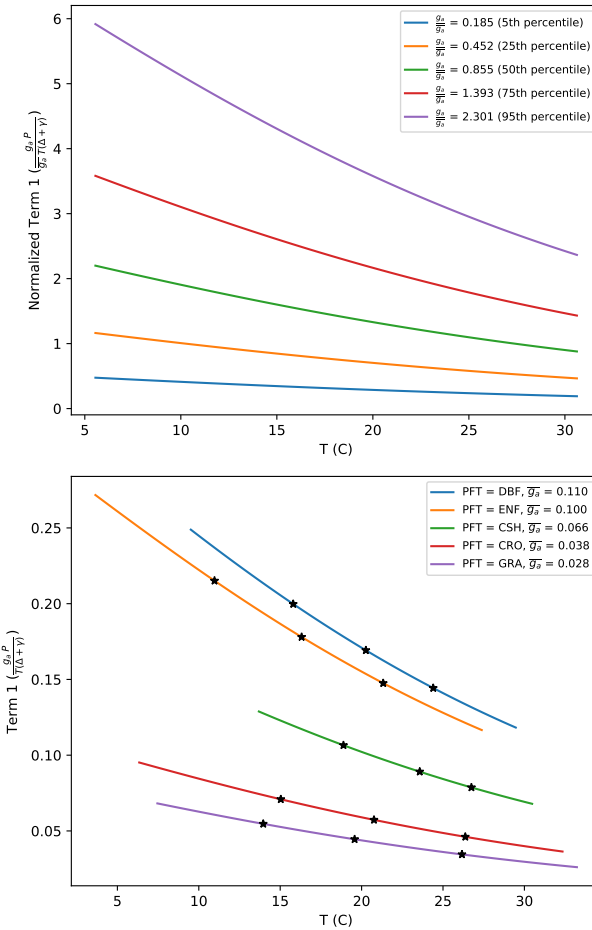
70 **Figure 1.** Plant functional type and location of sites used in analysis. Note should probably just split this
71 into 4 continents (US, Europe, Africa, Australia).



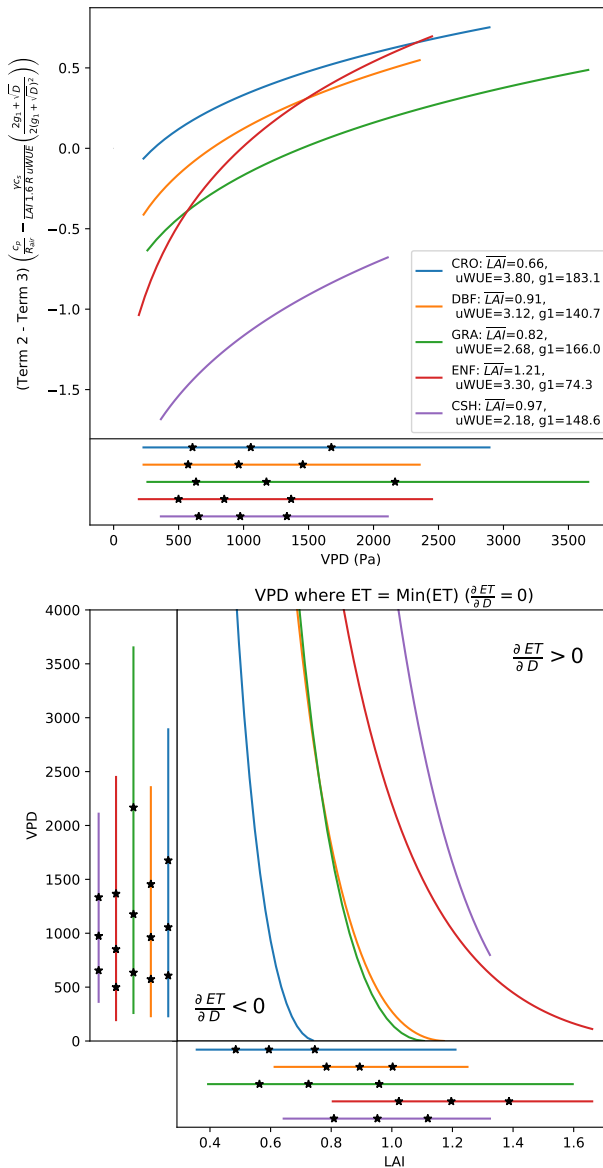
85 **Figure 2.** Histogram of LAI values calculated for each site and time according to Equation 8.
 86 The lowest and highest 5% are removed as outliers, as well as any values below 0. The curve is normalized such that its
 87 area is 1.



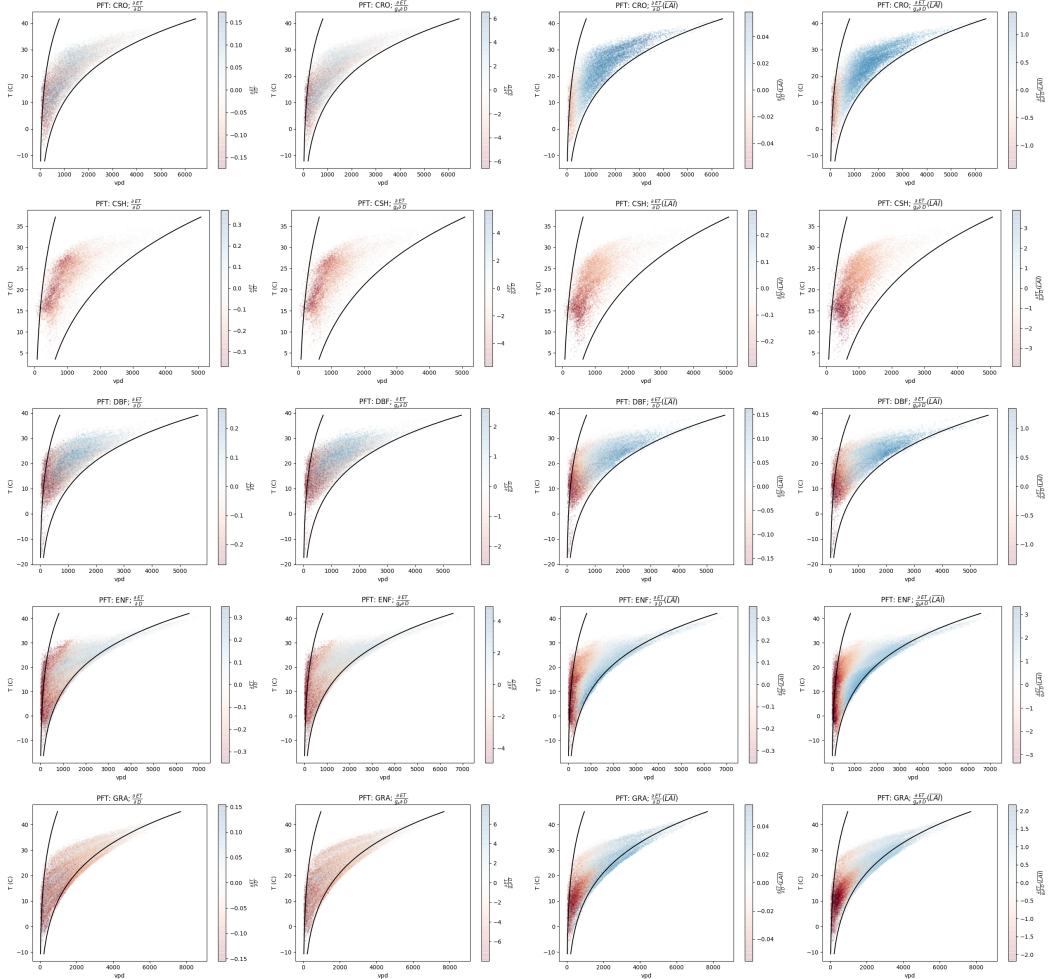
93 **Figure 3.** The joint distribution of D and LAI. LAI has only a weak dependence on D



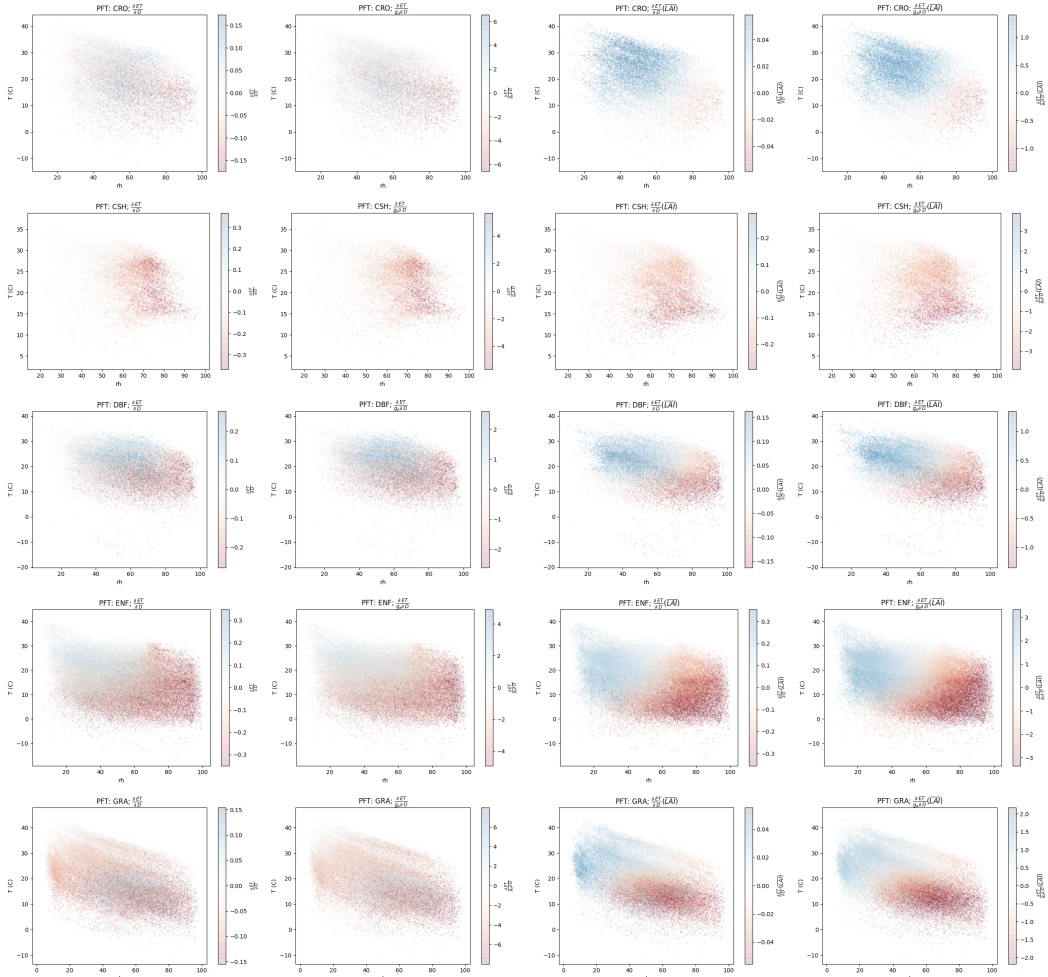
121 **Figure 4.** Primary sources of variability for Term 1. A) Variability within each PFT: Term 1 normalized by
 122 mean g_a for each PFT. B) Variability between each PFT: Term 1 evaluated at mean g_a for each PFT. Tempera-
 123 ture range is 5-95th percentile for each PFT. Additionally, stars denote the location of the 25th, 50th, and 75th
 124 percentiles.



135 **Figure 5.** Sources of variability for Term 2 - Term 3. Top: Term 2 - Term 3 as a function of VPD, with LAI
 136 held fixed at PFT averages. The observed range of VPD for each PFT is also shown below the x-axis. Line
 137 extent corresponds to 5th and 95th percentiles, while stars denote the location of the 25th, 50th, and 75th
 138 percentiles.
 139 Bottom: The location of the minima of ET, as a function of VPD and LAI. Lines and stars denote the distribu-
 140 tion of VPD and LAI next to axis, following the same percentiles as above.



196 **Figure 6.** Scatter plots of $\frac{\partial ET}{\partial D}$. Each row is a different PFT, and each column is a different quantity related
 197 to $\frac{\partial ET}{\partial D}$, as labelled: Column 1 - $\frac{\partial ET}{\partial D}$; Column 2 - $\frac{\partial ET}{\partial D}$ normalized by g_a ; Column 3 - $\frac{\partial ET}{\partial D}$ with LAI held
 198 fixed at PFT average; and Column 4 - $\frac{\partial ET}{\partial D}$ normalized by g_a and with LAI held fixed. For reference, lines
 199 corresponding to RH = 20% and RH = 90 % are drawn. Please note differences in the colorbar scale.



207 **Figure 7.** ****alternate Fig 06**** Scatter plots of $\frac{\partial ET}{\partial D}$. Each column
 208 is a different quantity related to $\frac{\partial ET}{\partial D}$, as labelled. If I end up using this, I could also draw on the curve of
 209 D_{ETmin} with \overline{LAI} .